

Article

Unveiling the Impact: Human Exposure to Non-Ionizing Radiation in the Millimeter-Wave Band of Sixth-Generation Wireless Networks

Naser Al-Falahy ¹ and Omar Y. Alani ^{2,*} ¹ Department of Electrical Engineering, University of Anbar, Ramadi 31001, Iraq; naser.falahy@uoanbar.edu.iq² School of Computing, Science, and Engineering, University of Salford, Manchester M5 4WT, UK

* Correspondence: o.y.k.alani@salford.ac.uk

Abstract: The investigation into potential hazards linked with millimeter-wave (mmWave) radiation is crucial, given the widespread adoption of body-centric wireless sensor nodes operating within this frequency band. This is particularly pertinent in light of its envisaged use for the upcoming 5G/6G networks and beyond. As 6G is anticipated to leverage a broad spectrum, including both sub-6 GHz and mmWave bands (30–300 GHz), concerns arise regarding increased human exposure to non-ionizing radiation (NIR). This work highlights the advantages of deploying 6G in the mmWave band, focusing on evaluating human body exposure to NIR interactions. Additionally, this research aims to address mmWave NIR exposure by introducing a Distributed Base Station (DBS) network. Utilizing low-power remote antennas to extend network coverage, the DBS architecture seeks to effectively minimize NIR's impact without compromising overall network performance. The findings underscore the significant potential of the DBS approach in mitigating NIR-related concerns associated with mmWave utilization in 6G networks.

Keywords: 6G; non-ionizing radiation; millimeter wave; distributed base station



Citation: Al-Falahy, N.; Alani, O.Y. Unveiling the Impact: Human Exposure to Non-Ionizing Radiation in the Millimeter-Wave Band of Sixth-Generation Wireless Networks. *Electronics* **2024**, *13*, 246. <https://doi.org/10.3390/electronics13020246>

Academic Editor: Dah-Jye Lee

Received: 2 December 2023

Revised: 28 December 2023

Accepted: 2 January 2024

Published: 5 January 2024



Copyright: © 2024 by the authors. Licensee MDPI, Basel, Switzerland. This article is an open access article distributed under the terms and conditions of the Creative Commons Attribution (CC BY) license (<https://creativecommons.org/licenses/by/4.0/>).

1. Introduction

To address the substantial surge in Global Mobile Data Traffic (GMDT), the development of the sixth-generation (6G) network has become imperative. According to Ericsson [1], global data traffic attributed to next-generation networks is experiencing a significant increase compared to the fourth-generation (4G) and other wireless networks, as illustrated in Figure 1.

The primary objectives of the fifth generation (5G) revolve around meeting heightened user demands, achieving extensive network capacity, and facilitating seamless connectivity for Internet of Things (IoT) applications [2]. In contrast, 6G is anticipated to be designed as an intelligent wireless network that leverages the power of Artificial Intelligence (AI); 6G is envisioned to usher in a paradigm shift toward the Metaverse, a space where reality can be shared between the cyber and real world, connecting and intelligently integrating all things [3].

To accommodate these highly demanding services, 6G is expected to operate at higher carrier frequencies in the millimeter-wave (mmWave) band, ranging from 30 to 300 GHz. This is due to the availability of considerable amounts of unused spectrum resources [4]. However, one crucial aspect that merits attention is the human body's exposure to Electromagnetic Field (EMF) radiation from mmWave base stations, leading to the generation of heat in human body tissues. This thermal effect becomes more pronounced as the frequency shifts from microwave to mmWave bands. Consequently, the mmWave band's limited penetration capability necessitates only a low level of EMF energy to induce heating in human tissues [5].

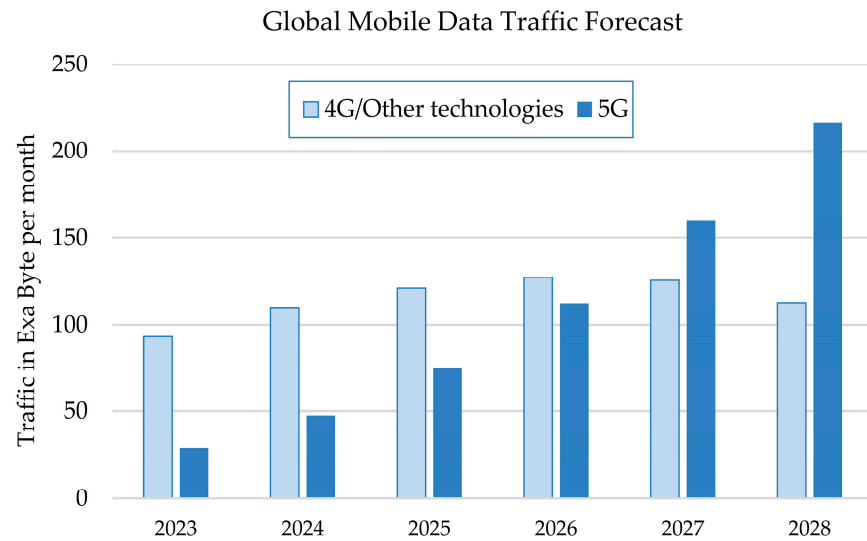


Figure 1. GMDT growth forecast.

Efforts such as the LEXNET research initiative [6] aim to minimize the radiation emitted by mmWave networks while upholding the Quality of Service (QoS) standards. Unlike X-rays and gamma rays, mmWave radiation falls under the category of non-ionizing radiation (NIR). This implies that it does not cause mutations or damage to human DNA, therefore posing no direct harm to the user’s biological system. However, the main concern remains the elevation of human tissue temperature due to EMF energy absorption [7].

The frequency band ranging from 30 to 300 GHz is commonly known as “Extremely High Frequency” (EHF) or “millimeter wave band”, whereas the 3 to 30 GHz band is known as “Super High Frequency” (SHF) or “centimeter wave band”. However, since both EHF and SHF have approximately the same propagation characteristics, the collective term “mmWave band” is employed, representing wavelengths spanning from 1 to 100 mm within the 3–300 GHz range [4]. For an illustration of the ionizing and non-ionizing spectrum, please refer to Figure 2.

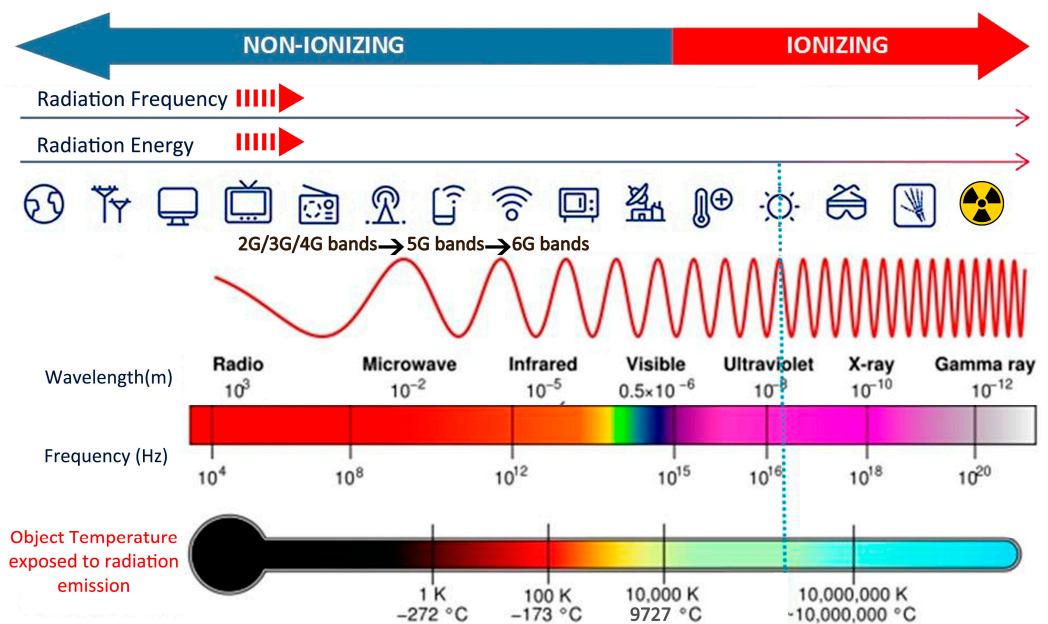


Figure 2. Ionizing and non-ionizing radiation spectrum.

The utilization of mmWave transmission in commercial applications must adhere to standard exposure guidelines [8,9]. To assess the exposure of Electromagnetic Field (EMF) energy at frequencies below 6 GHz, the Specific Absorption Rate (SAR) measurement is heavily relied on in the literature [5]. However, at higher carrier frequencies, there is a significant loss of penetration, limiting energy absorption primarily to the skin surface. Consequently, the radiation compliance above 6 GHz is evaluated using Power Density (PD) instead of SAR [5,6].

The investigation of NIR stemming from mmWave technologies is directly connected to EMF interaction with the biological systems of human beings. This research is of utmost importance due to potential public health concerns and the need to address health and environmental hazards [10,11]. Moreover, understanding exposure becomes even more crucial when considering mobile networks equipped with high-gain massive Multiple Input Multiple Output (massive MIMO) systems. In the context of telecommunications, massive MIMO, or large-scale MIMO, involves the implementation of a substantial number of antennas at the Base Station (BS) relative to those at the User Equipment (UE). This configuration enables massive MIMO to concurrently accommodate multiple UE channels, significantly enhancing the spectral efficiency of wireless networks to meet 6G and beyond network requirements [10]. Additionally, mMIMO offers increased degrees of freedom in interference coordination. However, to compensate for the increased path loss in the high-frequency band [12], mmWave BSs require massive antenna arrays to attain substantial gains. Consequently, the use of higher-gain arrays in mmWave BSs may lead to an increase in the heat sensation on human skin in the proximity of High-Power Node (HPN) base stations.

In the Distributed Base Station (DBS) architecture, the fronthaul link plays a pivotal role in transferring the data from the Remote Radio Heads (RRHs) back into the central unit known as the Base Band Unit (BBU). A significant advantage of this architecture is its seamless integration with the Cloud Radio Access Network (C-RAN), facilitating a powerful combination of cloud processing and the DBS architecture, significantly reducing computational complexity in wireless mobile networks and minimizing latency by leveraging the powerful capabilities of a vast number of Virtual Base Stations (VBSs) with parallel processing [13].

Furthermore, the adoption of C-RAN allows different networks to efficiently share their infrastructure (towers and equipment), fostering a more resource-efficient and collaborative ecosystem. In this regard, the research and industry should focus on unifying the digital markets of wireless networks, achieving multi-tenancy with major stakeholders [14]. The layout of the DBS architecture is illustrated in Figure 3, showcasing its structural components and connectivity.

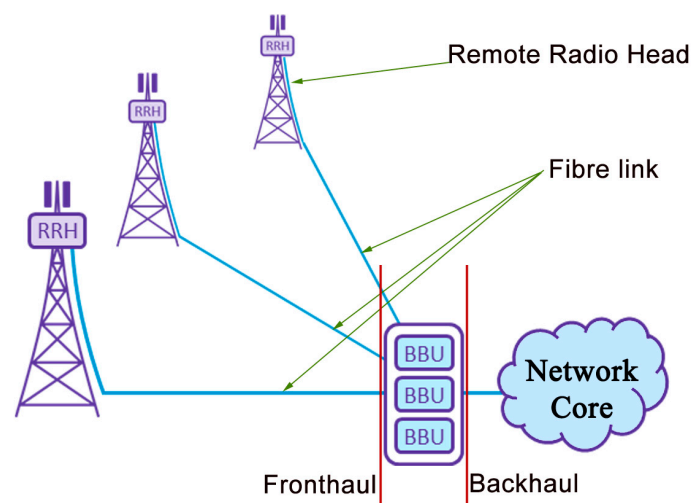


Figure 3. The DBS architecture.

Numerous studies have been dedicated to investigating the interaction of NIR from the mmWave band with the human body. For instance, the authors of [15] explored the effects of Maximum Permissible Exposure (MPE) levels at 60 GHz (free licensed band) on human cell membranes using Low-Power Nodes (LPNs) with a power density of 10 to 100 mW/cm². In [16], researchers delved into the thermal response of human tissue exposed to the radiation of mmWave transmitters, concluding that a steady-state temperature (ssT) increase occurs in human cell membranes when a base station radiates at certain power levels.

Rappaport et al. [7] considered the impact of NIR on the human body and suggested that measuring the ssT is preferable to power density (PD) when mmWave transmitters are in close proximity to the human body.

In terms of specific exposure scenarios, ref. [17] investigated near-field radiation from transmitting nodes at mmWave frequencies, demonstrating significant radiation absorption on the user's ear during calling and on their fingers during browsing. Electromagnetic field (EMF) radiation in the mmWave frequencies is evaluated in [18]; the authors conducted empirical assessments at 28 GHz using horn and path antenna types, evaluating the power density based on the E-field. The resultant heat increase due to the exposure to EMF within the 6 GHz to 1 THz range was studied in [19] across different exposure scenarios.

Regarding human tissue proximity to 6G-transmitting nodes at mmWave frequencies above 24 GHz, ref. [20] explored the absorption of EMF energy, concluding that the heat effect was negligible in comparison to public safety margins. Additionally, the work in [21] conducted resonant heating experiments at 24 and 28 GHz on individual insects, presenting exposure impact results and suggesting that NIR exposure could alter termite behavior and potentially be lethal to them. Furthermore, the impact of NIR on the human body was analyzed and demonstrated in [22], where safety standards were examined and benchmarked in the best healthcare services of different countries.

The development of the Reconfigurable Intelligent Surface (RIS) can play a major role in network design and beamforming selection. RIS is a surface with a massive number of reflectors; these reflectors can potentially impose an amplitude and phase shift to adjust the coefficients of the incident wave [23]. In this context, ref. [24] demonstrated how RIS can be used as a malicious attack by modifying the incident signal so that it provides destructive beamforming at the target device. This can result in significant fading in the received signal, and in the case of mmWave, there is no gain from using beamforming, there is only the "pain" of exposure to mmWave. On the other hand, RIS can be used to provide robust beamforming, which can help suppress jamming [25].

Furthermore, reference [26] presented an overview of radiation exposure and the interaction of EM waves with the human body. The study suggested that in order to minimize the radiation effect, it is necessary to work on a heterogeneous network with reduced transmit power using femto and pico base stations, especially at the 20–70 Hz band. Meanwhile, in [27], a radiation reduction mode is proposed, particularly for mmWave, through the adoption of Non-Orthogonal Multiple Access (NOMA) to replace the Orthogonal Frequency Division Multiple Access (OFDMA), and digital beamforming and MIMO coordination to suppress radiative interference in the controlled area. A two-dimensional computational analysis of the Specific Absorption Rate (SAR) was conducted by [28]. The author examined the collected temperature on the human body using non-ionizing and ionizing radiation and showed how the duration of exposure can contribute to a greater temperature increase. A thermal radiation mode is suggested in [29] for networks operating at the mmWave band, with a special focus on elevated heat in the human body. The study is based on SAR and power density figures, aiming to reduce the radiation of wireless communication networks to increase the safety and reliability of next-generation networks.

Additionally, the radiation exposure for both downlink and uplink transmission is studied and analyzed in [30]. The authors quantified the radiation through the use of electric and magnetic field strength in their calculation of power density and suggested

a power control scheme as a way to suppress the radiation in both uplink and downlink transmission. A detailed survey on radiation exposure and its concern to public health is presented in [31]; the authors also provided experimental outdoor analysis of the exposure to the electric field at different locations using a dosimeter in downlink mode.

This paper focuses on the requirements of the regulations concerning NIR within the mmWave band. Specifically, it centers on the implementation of LPN as a 6G-transmitting node in a DBS architecture, employing multiple RRHs to replace High-Power Nodes (HPNs) like mMIMO arrays, which may lead to increased radiation exposure in the proximity of HPN deployments. HPN mMIMO systems rely on high-gain antenna arrays to enhance the communication link and compensate for the considerable path loss and penetration loss in mmWave propagation. In contrast, the LPN approach in a DBS architecture employs spatially distributed RRHs (which consequently make the network nodes much closer to users), effectively mitigating the excessive path loss. The DBS network can significantly decrease the NIR exposure rate due to its low-power nature compared with massive MIMO and beamforming. Therefore, a DBS architecture and mmWave network fit well as a promising way to reduce the impact of NIR in mobile networks.

This work is motivated by the introduction of a Fog Radio Access Network (F-RAN) in next-generation mobile networks to achieve Ultra-Reliable Low-Latency Communication (URLLC) [32,33]. The massive distribution of Virtual Baseband Units (VBU) in F-RAN in the form of an access point or RRHs for interference coordination and resource management is similar to the architecture of a DBS network. DBS F-RAN, in this work, is envisioned as the future network paradigm in the mmWave band and adopted as a novel way to suppress the potential hazard of NIR in mmWave 6G networks.

The rest of this paper is structured as follows: Section 2 presents a discussion on the exposure regulations pertinent to mmWave frequencies. In Section 3, an in-depth exploration of mmWave takes place, which includes an analysis of path loss and foliage loss models. Moving on to Section 4, the paper presents the metrics employed to assess NIR exposure. The network model and simulation settings are the subject of Section 5. Section 6 involves a comprehensive examination of the simulation results. Finally, Section 7 draws conclusions based on the findings presented throughout the paper.

2. Exposure Regulations at mmWave Frequencies

The guidelines prescribed by the Federal Communications Commission (FCC) encompass specific limits for MPE concerning electric and magnetic field strength, as well as power density for transmitting nodes operating within the range of 300 kHz to 100 GHz [34]. Additionally, the Institute of Electrical and Electronics Engineers (IEEE) has developed standards governing exposure to NIR. These standards explicate the allowable duration and quantity of exposure for individuals in both controlled and uncontrolled areas. These restrictions are outlined in the IEEE C95.1-2005 [8]. Table 1 provides a summary of the NIR exposure limits based on averaging time, in accordance with the IEEE standards. Contrasting this, the International Commission on Non-Ionizing Radiation Protection (IC-NIRP) standard sets restricted levels for power density at frequencies ranging from 10 to 300 GHz. For the general public, the power density restriction is set at 10 W/m^2 , while for the occupational group, it is set at 50 W/m^2 (Table 5 in [9]).

Table 1. MPE limits—average PD for uncontrolled and controlled areas with averaging time.

Frequency (GHz)	Power Density (Controlled Envir.) “Upper Tier” in W/m^2	Power Density (Uncontrolled Envir.) “Lower Tier” in W/m^2
3 to 30	100 in avg. time = $19.63/f^{1.079}$ min	10 in avg. time = $150/f$ min
30 to 100	100 in avg. time = $2.524/f^{0.476}$ min	10 in avg. time = $25.24/f^{0.476}$ min

where f represents the frequency in GHz.

Moreover, the IEEE standard allows for a relaxation of MPE power density when considering exposure to any part of the human body. In controlled environments, the power density must not extend $200(f/3)^{1/5}$ W/m² for 3 to 96 GHz and 400 W/m² for the frequency band of 96 to 300 GHz. In the case of uncontrolled environments, the standard limits the power density level below $18.56(f)^{0.669}$ W/m² for the 3 to 30 GHz band and 200 W/m² for the 30 to 300 GHz band [7,8].

3. The mmWave Band

This section presents an overview of the potential bands for 6G networks and assesses the migration to mmWave frequencies. Within the sub-6 GHz bands, approximately 2.5 GHz of licensed bandwidth is designated, with a significant portion allocated at 3.5 GHz. However, when considering the mmWave band, the responsible regulatory bodies for spectrum allocation, such as the FCC in the United States [35] and the International Telecommunication Union-Radio (ITU-R) [36], have released numerous bands.

The mmWave bands have been designated at frequencies ranging from 28 to 30 GHz, 38 to 40 GHz, and a free-licensed band extending from 57 to 71 GHz, providing a valuable 14 GHz of contiguous band. Notably, this allocation represents 15 times the unlicensed spectrum of Wi-Fi [37]. Additionally, a 12.9 GHz band is located at 71–76 GHz, 81–86 GHz, and 92–95 GHz [38,39]. Furthermore, in the UK, Ofcom has released the 26 GHz frequency band, spanning from 24.25 up to 27.5 GHz, for potential 6G utilization [40]. In China, considerations are being made for 45 GHz bands for both licensed and unlicensed wireless networks. For bands above 100 GHz, ITU has released a wide bandwidth of more than 20 GHz of unlicensed spectrum for wireless communication and applications [41,42]; this spectrum will shape the future of wireless communications [43]. For more details about the potential bandwidth allocation for 6G, please refer to Table 2.

Integrated satellite–terrestrial networks can also share the mmWave bandwidth with mobile networks; these satellites adopt digital beamforming to form multibeam transmission [44]. To provide a visual representation, Figure 4 illustrates the candidate bandwidths for 6G, encompassing the various mmWave bands and their allocated frequencies [10].

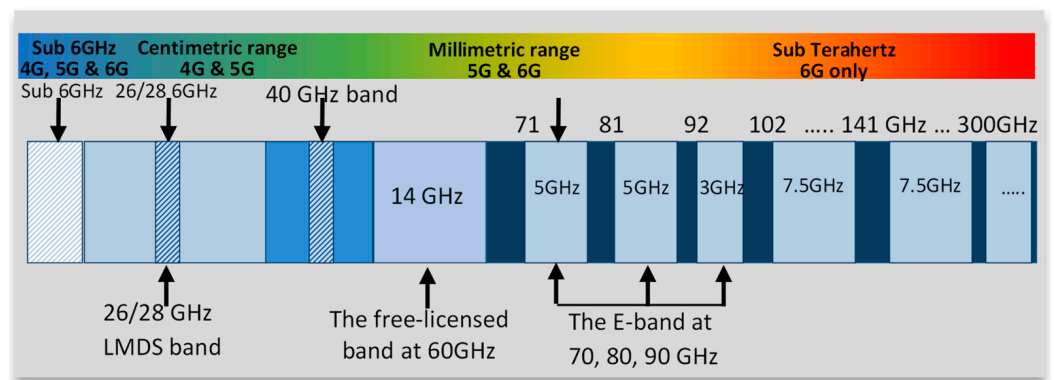


Figure 4. Next-generation candidate spectrum.

Table 2. Potential frequency band for 5G/6G networks.

	Sub-6 GHz Band [4,45]					Centimeter- and Millimeter-Wave Band [4,45–47]										Complementary Sub THz Band [41,42]			
Frequency in (GHz)	1.8	2.1	2.6	3.3	5	6.425–7.125	7–24	26	28	40	60	70	80	90	102–109	151.5–164	167–174.8	209–226	252–275
Network Generation	Other technologies/4G/5G					5G/6G										6G only			

The following path loss and foliage loss models are both adopted in the simulation as part of the parameters of the simulation setting and the calculation of the performance metrics to evaluate the DBS LPN and HPN network models.

3.1. The mmWave Path Loss

The mmWave channel measurements conducted in [12,48] illustrate the highly sensitive nature of mmWave to blockages, resulting in distinct Line-Of-Sight (LOS) and Non-Line-Of-Sight (NLOS) path loss characteristics. During transmission, mmWave signals suffer from substantial penetration loss when passing through solid materials. Furthermore, heavy rain can lead to significant attenuation as a result of signal scattering because the size of raindrops is of a similar size to mmWave wavelengths [47]. Consequently, the LOS link is limited due to the presence of obstructions. On the other hand, NLOS transmission occurs due to reflected waves from blockage surfaces, typically resulting in weaker signals but still contributing to providing coverage for users in shadowed areas [48].

The path loss exponent for LOS transmission is similar to that of free space and is represented by a value of 2 [49]. However, for the NLOS link, the path loss exponent has been measured to be larger than the LOS exponent, with values of 3.86 at the University of Texas, Austin campus, and 5.76 at NYC downtown [12,49]. Additionally, the 3rd Generation Partnership Project (3GPP) released a path loss model for frequencies ranging from 0.5 to 100 GHz [50]. Consequently, the path loss between a 6G-transmitting tower and a receiving device, as described in this context, is defined for LOS and NLOS by the model proposed in [50] as follows:

$$L_{\text{LOS}} = 32.4 + 20\log_{10}(f) + 21\log_{10}(d) \quad (1)$$

$$L_{\text{NLOS}} = 32.4 + 20\log_{10}(f) + 31.9\log_{10}(d) \quad (2)$$

where f is the link frequency in GHz, and d is the distance between a transmit antenna and a mobile antenna in meters, as shown in Figure 5. A path loss map is shown in Figure 6 for Co-located Base Station (CBS) and DBS networks, in terms of the Signal-to-Interference-plus-Noise Ratio (SINR) [51].

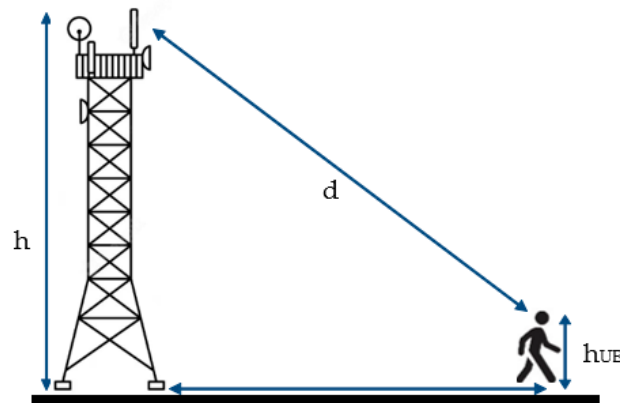


Figure 5. The path loss model.

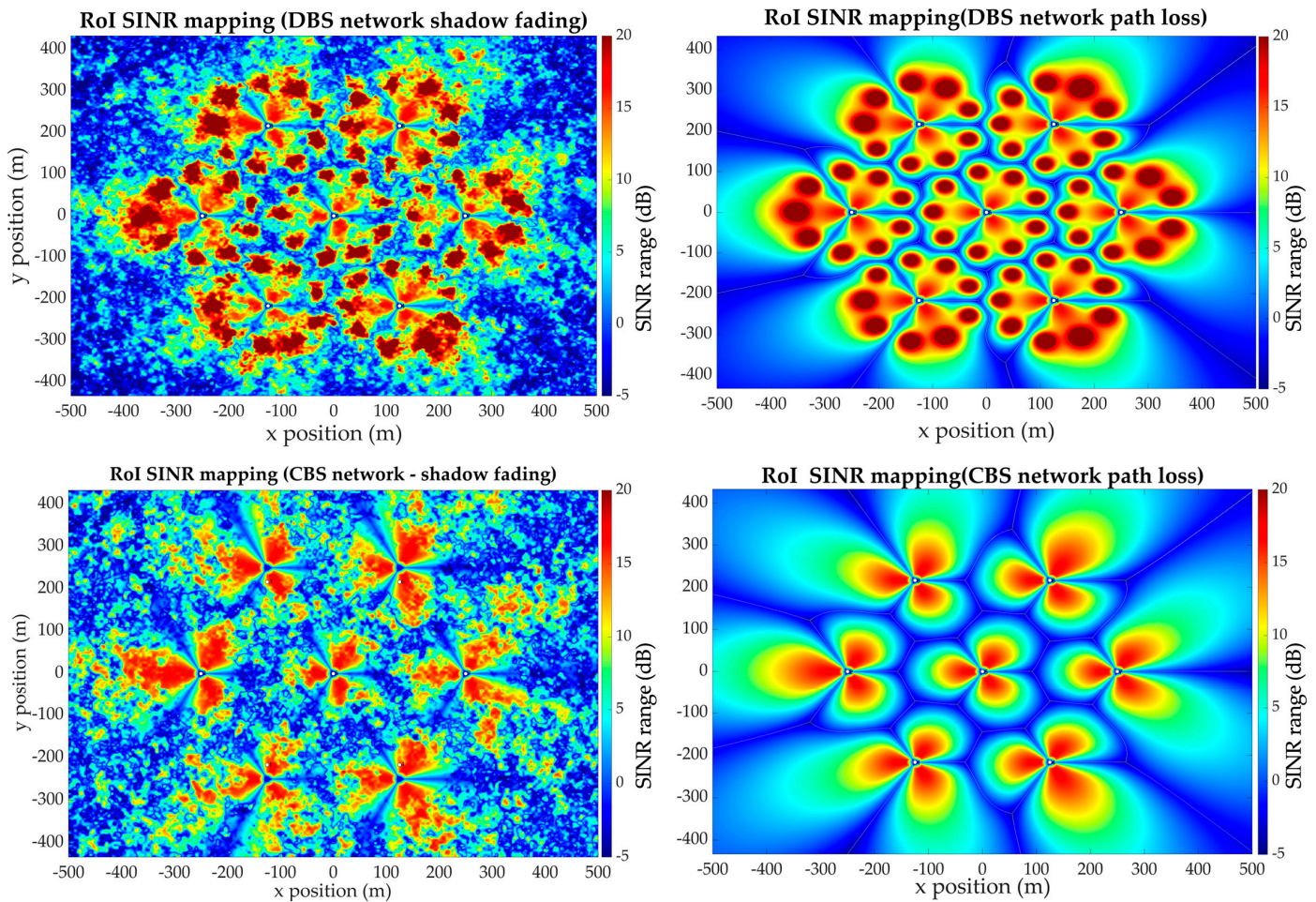


Figure 6. SINR mapping with/without shadow fading, the DBS architecture (upper snap), and CBS architecture (lower snap), where the color bar represents the range of SINR in dB.

3.2. Foliage Loss

The Weissberger model has been used in this work to define the signal propagation through vegetation in mmWave networks [52]. The Weissberger foliage loss is described by the following:

$$L_f = 0.45 f^{0.284} (d_f) \text{ for } 0 \leq d \leq 14 \text{ m} \tag{3}$$

$$L_f = 1.33 f^{0.284} (d)^{0.588} \text{ for } 14 \leq d \leq 400 \text{ m}$$

where f represents the center frequency in GHz, applied for 230 MHz to 95 GHz, and d is the depth of the foliage in meters. The overall propagation loss is equal to the path loss (described earlier) added to the Weissberger foliage loss:

$$L_T = P_L + L_f \tag{4}$$

The ITU foliage model is a different model for characterizing foliage loss, which was developed by (CCIR Rpt 236-2) [53]. The ITU foliage loss model is defined as follows:

$$L_F = 0.2 f^{0.3} d^{0.6} \tag{5}$$

where L_F is the foliage penetration loss in dB, f is the designated frequency in MHz, and d is the depth of the foliage in meters. In Figure 7, we present the plotted foliage loss for both the ITU and Weissberger models, considering two different foliage depths: 3 m and 15 m. The graph illustrates that the ITU model yields relatively consistent results with

minimal variation when compared to the Weissberger model. The foliage loss values for the specified models and foliage depths are depicted, providing valuable insights into the performance of the respective models under different foliage conditions.

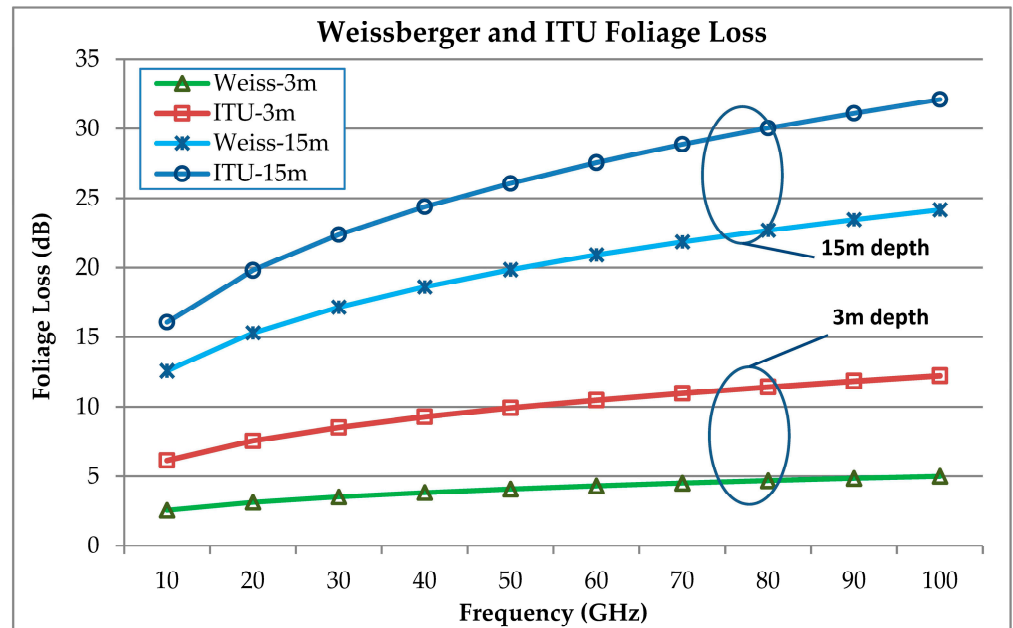


Figure 7. Weissberger and ITU foliage loss in mmWave for different foliage depths.

4. Radiation Metrics

The energy of a photon can be described by [54]:

$$E = hf = \frac{hc}{\lambda} \tag{6}$$

where E is the photon energy, h is Plank’s constant, c is the speed of light, and λ is the designated wavelength. The energy of a photon in the mmWave band is 0.012 up to 1.2 milli-electron volts (meV). The mmWave radiation metrics are as follows [55]:

4.1. Specific Absorption Rate (SAR)

Specific absorption is the rate at which energy is absorbed by a mass within a given volume, considering its density. It is the time derivative of the increased absorbed energy by the mass. SAR is expressed in the SI unit of Watts per kilogram (W/kg), where

$$SAR = \frac{P_i}{m_i} = C_h \left. \frac{dT}{dt} \right|_{t=0} \tag{7}$$

where P_i is the power of the incident wave, and m_i is the mass of the body. Unlike the power density, SAR calculation considers the sample’s physical properties. SAR is also described by the electric field:

$$SAR = \frac{\sigma |\vec{E}|^2}{\rho_m} \tag{8}$$

where σ is the tissue conductivity, and ρ_m is the tissue mass density. Furthermore, SAR can also be described by the temperature increase:

$$SAR = C_h \left. \frac{dT}{dt} \right|_{t=0} \tag{9}$$

where C_h is the heat capacity in $\left(\frac{J}{kgC^\circ}\right)$, T is the temperature, and t is the exposure duration.

4.2. Power Density

Power density is the primary metric of radiation used by international standards and guidelines governing mmWave frequencies. The power density can be defined as follows:

$$PD = \frac{P_i}{S_a} = |\vec{E} \times \vec{H}| \quad (10)$$

where S_a is the area exposed to the incident wave, and \vec{E} and \vec{H} are the vectors of the electric and magnetic fields.

4.3. Steady-State Temperature (ssT)

The ssT is an important measure, especially in scenarios involving medium- to high-power radiation exposures at mmWave frequencies [16]. In such cases, ssT is considered to be preferable over SAR and power density, particularly when evaluating devices positioned close to the human body, such as sensors at mmWave frequencies. ssT offers valuable insights into the potential thermal effects on biological tissues, making it a relevant metric for assessing the safety and health implications of mmWave radiation exposure.

5. Network Model

This section presents the network models used in this work, namely, CBS and DBS network models, and illustrates the simulation settings and parameters used to produce the results. In the context of the Radio Access Network (RAN), the typical architecture of wireless networks involves a single Base Station (BS) providing coverage and resources to users. This traditional network implementation often consists of a three-sector node, where the BS employs directional antennas in three directions, located at the BS site. This architecture is referred to as CBS network architecture.

However, an alternative approach is the DBS architecture. In this architecture, the BS is divided into two units: the central unit known as the BBU, and RRH units mounted on towers situated at a distance far from their corresponding BBUs. High-speed fiber-optic links connect the RRHs to their BBUs, serving as both the power supply for the RRHs and the medium for carrying signaling [13]. The DBS architecture inherently represents the native structure of C-RAN networks, and the RRHs collect and relay the traffic back to the local VBS to handle complex processing through powerful cloud computing.

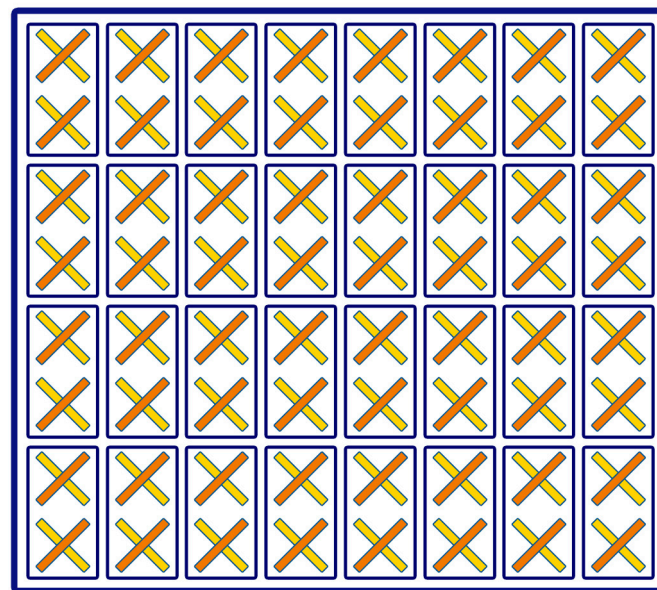
The simulation parameters are shown in Table 3. The distributed RRHs share resources with users in close proximity. The RRHs are connected to their respective BBUs through high-bandwidth fiber links, also known as fronthaul links. The BBUs, in turn, establish backhaul links to the C-RAN cloud, enabling the processing of substantial data from the RRHs. The user distribution is modeled as a uniform distribution, with more than 100 users in the Region of Interest (RoI).

In this simulation, HPN employs a single BS that implements a large-scale MIMO array antenna, consisting of 128 antenna elements arranged in an 8×8 configuration with dual polarization, as depicted in Figure 8. The gain of the array is 30 dB, and it transmits at 46 dBm. Additionally, the LPN in DBS network architecture has a 20 dB gain and transmits at 30 dBm. The RRHs are distributed 100 m away from the BBU. The area of the simulation measures $300 \times 300 \text{ m}^2$. HPN and LPN transmitters are set at a 10 m height, and all UEs at a 1.5 m height.

Table 3. Network parameters.

Parameters	Value
Link	Downlink
Designated frequency	28 GHz
Path loss model	As per 3GPP Report 38.901 [50]
Foliage loss model	Weissberger model [52]
Bandwidth	Up to 500 MHz
Tx Power	30–46 dBm
RRH gain	15 dB
MIMO array gain	30 dB
RRH distribution	3 per BBU
Antenna type	SISO and MIMO
Tx height	10 m
Rx height	1.5 m
MIMO	128 elements
Polarization	−45/45 X-POL
RoI	300 × 50 m Street Canyon
MPE model	IEEE C 95.1-2005 model

✕ is -45/45 X polarized antennas
 Array gain : 30 dB , 128 elements

**Figure 8.** HPN 128-element massive MIMO simulation with ± 45 antenna polarization.

To carry out the simulation, a test area is selected and designed as a street canyon, as depicted in Figure 9. The street canyon exhibits a width of 50 m and is flanked by high-rise buildings on both sides. Two types of transmitters are employed for the investigation: an HPN with a massive MIMO array containing 128 elements, and a Low-Power Node with a 4×4 MIMO configuration. All transmitters are at a height of 10 m, simulating a small-cell deployment scenario. The receivers in this study, representing the mobile users, are uniformly distributed along the street at a height of 1.5 m.

Through this simulation setup, the study aims to gain insights into the potential exposure levels to electromagnetic radiation experienced by end users in the vicinity of HPN sources compared to the LPN deployment. By considering the specific radiation characteristics and deployment scenarios, this research seeks to provide valuable guidance for ensuring the safety and efficiency of 6G network deployments.

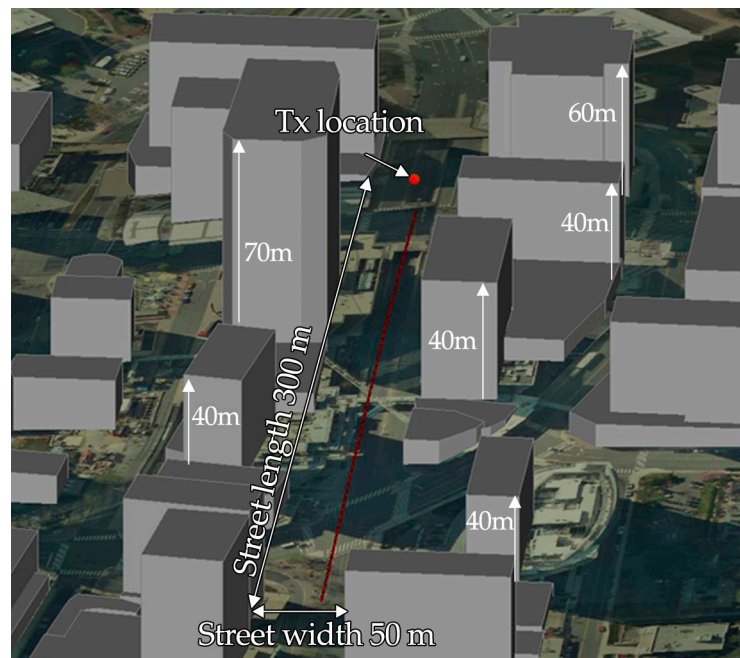


Figure 9. The simulation area (RoI), 3D model of street canyon.

Power density has been employed as the second measure to characterize the impact of NIR from mmWave wireless networks. Power density serves as a crucial metric for assessing the level of electromagnetic energy exposure in the surrounding environment and is utilized to evaluate the potential NIR effects of mmWave communication systems. By using power density as a key parameter, this study aims to gain valuable insights into radiation levels and their potential implications on human health and safety, contributing to a comprehensive understanding of the mmWave network's impact on the electromagnetic environment. The general calculation of MPE is derived from the Friis equation [33]:

$$S_r = \frac{P_t G_t}{4\pi r^2} \quad (11)$$

where S_r represents the PD, P_t is the transmit power, G is the gain of the antenna, and r represents the Tx–Rx separation. In this context, knowing the power gain of the transmitter, the MPE can be easily calculated at any distance.

6. Results and Discussion

This section demonstrates the results and their corresponding discussion and justifications. The section starts with the default CBS network, to present the impact of HPN nodes in terms of power density. After that, the DBS network results are shown to compare the results and emphasize the importance of the DBS network over the CBS network.

This study adheres to the IEEE controlled area guidelines for “upper-tier” exposure, as outlined in the IEEE C95.1-2005 standard. It investigates radiation hazard levels with distance from the transmitting HPN– and LPN–DBS transmitting sources to outdoor users of 6G. Such information is crucial for the effective planning and optimization of 6G networks, especially in cases where an HPN with a very large-scale antenna array is utilized.

6.1. HPN with CBS Architecture

In this paper, the HPN is depicted as a massive MIMO equipped with a 128-antenna array. In this paradigm, the base station transmits at 46 dBm. The received power results are presented in Figure 10, showcasing that in the massive MIMO scenario, very high-power levels are reported compared to the DBS network. This is a consequence of the

substantial number of antennas in the massive MIMO base station in contrast to the UE. The increased antenna gain effectively compensates for the high path loss at mmWave frequencies, resulting in a notable reduction in the exhibited path loss, as illustrated in Figure 11. This enhancement in gain achieved by the massive number of antennas in the HPN significantly contributes to the successful mitigation of challenges posed by mmWave propagation and ensures robust network performance.

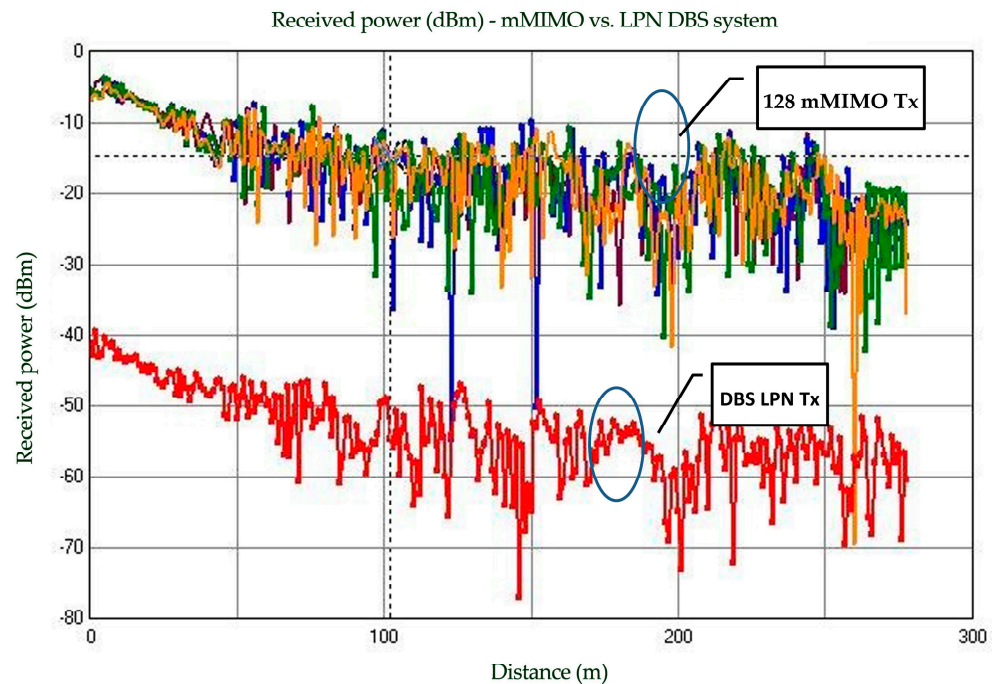


Figure 10. Received power (dBm) for mMIMO and DBS. Where colors represent different signals from the massive MIMO array.

However, the use of massive MIMO has significantly increased the power density in the vicinity of the base station transmitter. As a result, high figures for MPE levels are reported, particularly for users located within the radiation area. These users may experience elevated temperature increases in their eyes and skin tissues due to exposure to mmWave NIR.

Figure 12 illustrates the power density measured in W/m^2 received by UEs in relation to the hazard threshold according to the regulations of the IEEE and the ICNIRP. The findings show that UEs in close proximity to the massive MIMO array may be exposed to mmWave NIR, potentially leading to heat increases in their body tissues, particularly in the area below 200 m. This area (<200m) where the power density (blue line) crosses the safety standards (red line) can pose a significant hazard to living beings and needs to be addressed. Prolonged exposure to NIR in these areas can lead to even worse diseases such as tissue damage and other related consequences.

It is important to emphasize that these radiation exposure results are based on the assumption of stationary transmitters and receivers. In scenarios where users are moving at higher speeds, lower figures of exposure are expected due to the dynamic nature of the wireless communication system. Nevertheless, this study highlights the need for careful consideration of power density levels in close proximity to massive MIMO arrays operating at a high frequency to ensure compliance with safety standards and mitigate potential health risks for users.

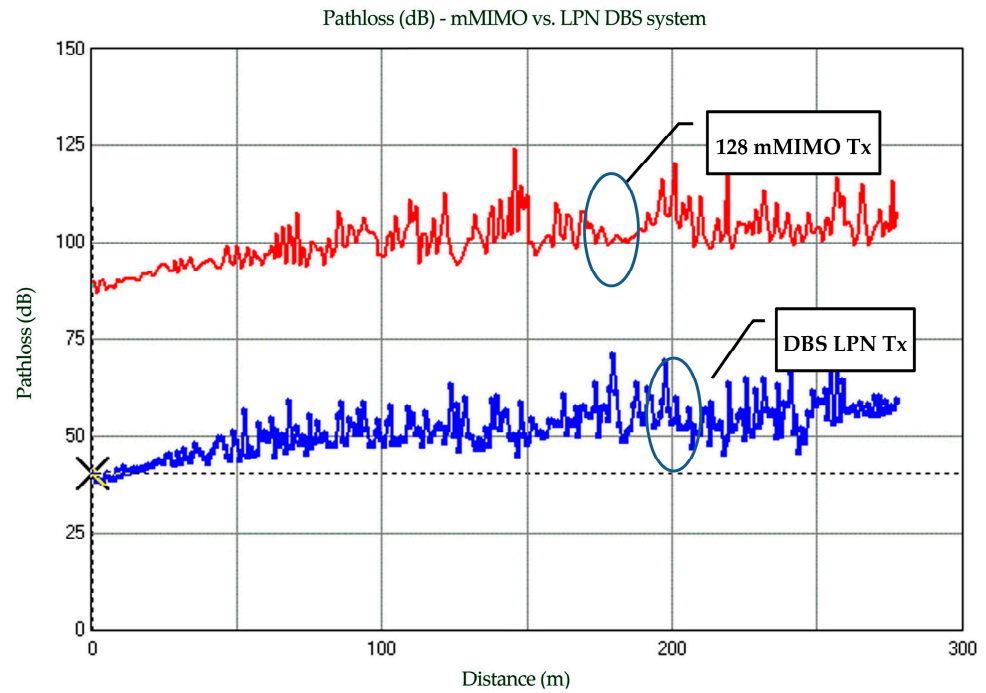


Figure 11. Path loss (dB) for mMIMO and DBS base station.

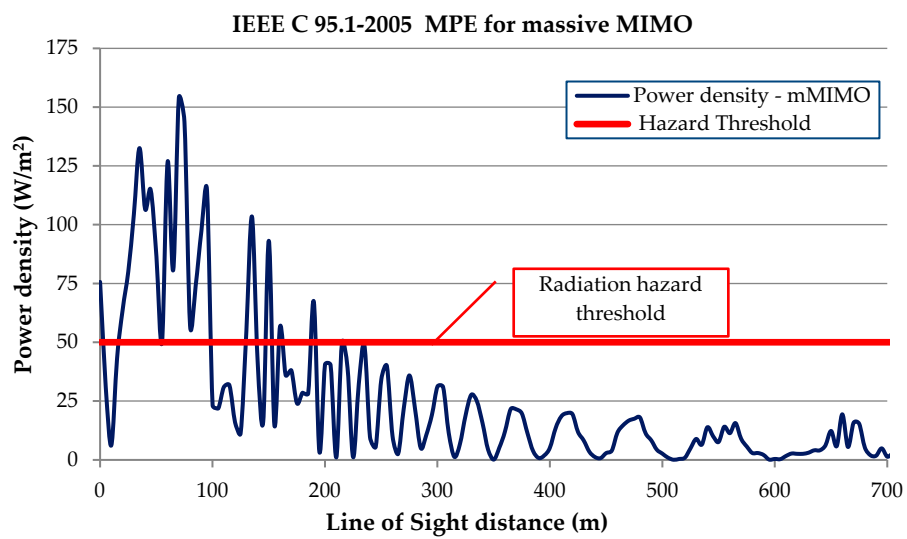


Figure 12. IEEE C 95.1-2005 power density for massive MIMO.

6.2. LPN with DBS Architecture

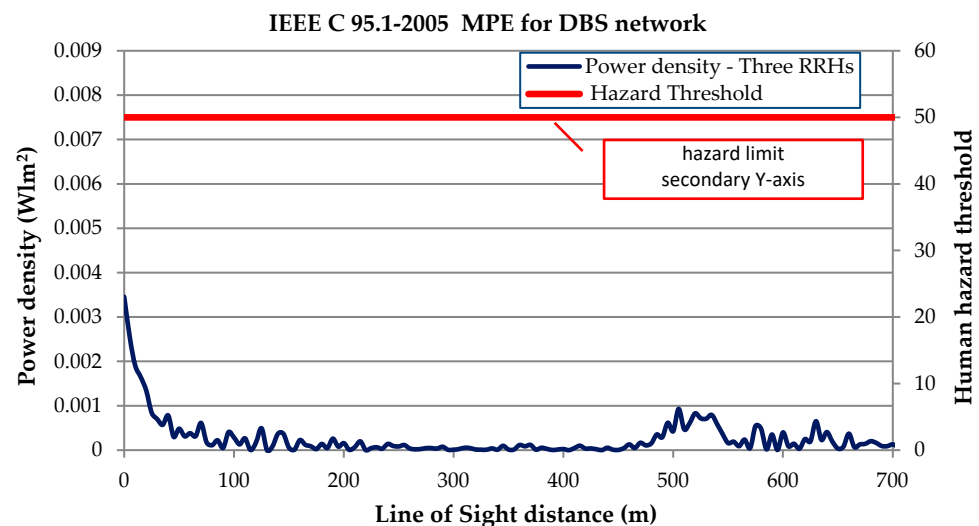
The architecture of the DBS network proposes an efficacious method to augment network coverage within the mmWave band. The DBS approach uses dispersed RRHs as a compensation measure for the escalated path loss occurring at mmWave frequencies. By positioning RRHs in closer proximity to end users, the signal pathway and corresponding path loss are minimized. This strategy enhances spectral efficiency and fosters a more equitable allocation of resources [51,56]. Furthermore, the DBS architecture holds the potential to amplify LoS signal coverage through the strategic spatial distribution of remote antennas, embodied in RRHs. The dispersed configuration of RRHs mitigates the effect of shadow fading, facilitating a larger proportion of UEs to maintain LoS connectivity, as delineated in Table 4. In the corresponding simulation, 1100 UEs were deployed to contrast the coverage and outage probability metrics of DBS and CBS architectures.

Table 4. Coverage probability of HPN and LPN.

Network Type	HPN-CBS	LPN-DBS
All UEs	1000	1000
LOS + NLOS	880	968
Outage UEs	120	32
Prob. of Coverage	88%	96.8%

In this study, an LPN with a transmit power of 30 dBm in a DBS network architecture is compared with the massive MIMO architecture. Three RRHs are employed in the DBS scheme to provide a coverage solution. In the DBS network, the RRHs can be powered with green energy sources, promoting a cleaner and more sustainable 6G network. The DBS architecture exhibits significantly reduced received power without compromising the QoS provision.

Table 4 demonstrates an improvement in the probability of coverage in the DBS network. The transmit power is distributed over three RRHs as well as the BBU. Therefore, the power density is substantially decreased, and no reports of increased radiation are observed in the DBS system. Figure 13 illustrates the average power density with respect to distance; the results are averaged for all distributed RRHs in the area of interest. The MPE of the aggregated signal power density does not pose hazard figures, alleviating potential concerns related to radiation exposure.

**Figure 13.** IEEE C 95.1-2005 MPE—DBS architecture.

The DBS architecture, with its distributed RRHs and reduced power density, proves to be a promising solution for achieving efficient mmWave network coverage while ensuring compliance with safety regulations and environmental considerations.

The implementation of the DBS architecture has successfully achieved a reduction in radiation exposure without compromising the overall network performance. To demonstrate the performance of both the traditional CBS and DBS networks, a system-level simulation tool was utilized in the 26 GHz “pioneer band” (a frequency band from 24.25 up to 27.5 GHz), specifically designed for high data throughput applications and services, released by Ofcom—London, UK.

In the system-level simulation, the advantages of the DBS over the CBS architecture were further analyzed. The simulation results illustrate that the DBS architecture exhibits superior spectral efficiency compared to the CBS network. This improvement can be attributed to the distribution of RRHs in the designated areas, thereby enhancing the signal path gain. As a result, the DBS network achieves better spectral efficiency, leading to an enhanced user experience in terms of average user throughput, as shown in Figures 14 and 15.

These figures show the Cumulative Distribution Function (CDF) of spectral efficiency and data throughput, respectively.

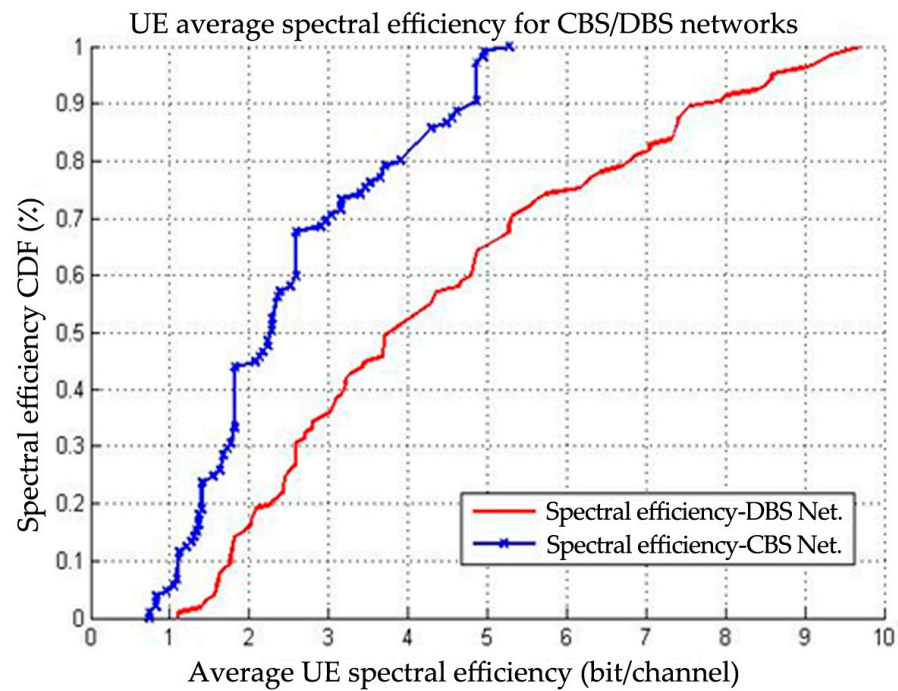


Figure 14. Spectral efficiency of CBS and DBS networks.

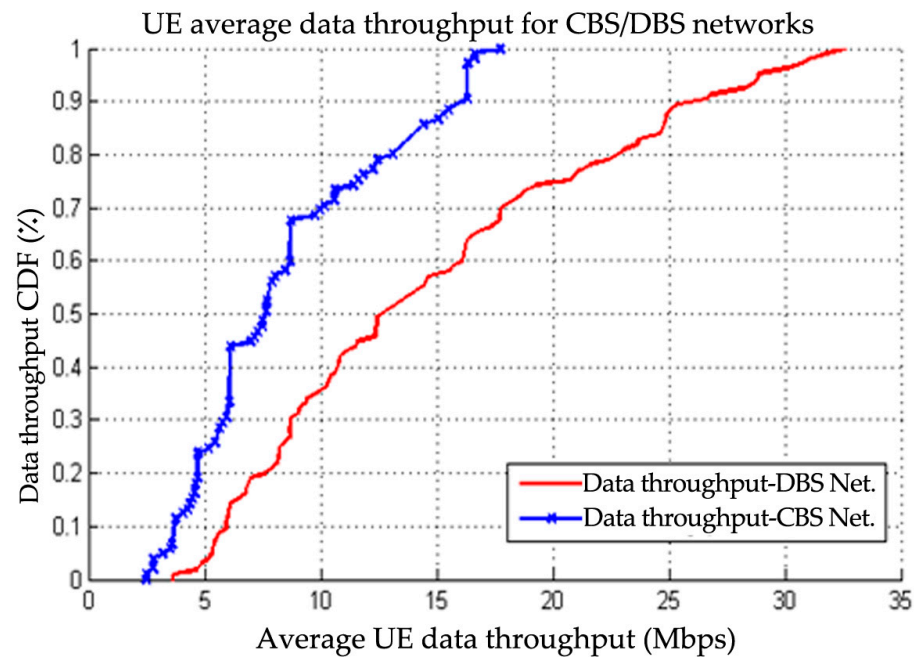


Figure 15. Data throughput of CBS and DBS networks.

The improved spectral efficiency and enhanced user throughput in the DBS environment highlight the potential benefits of this architecture in high data rate demand scenarios. The DBS network’s ability to capitalize on the spatial distribution of RRHs, reducing path loss and enhancing signal gain, contributes to the overall optimization of the 6G network performance, making it an attractive solution for future mmWave deployments.

7. Conclusions

This study focused on evaluating the performance of a DBS network at mmWave frequencies as the envisioned architecture for a 6G network. The evaluation encompassed reducing Non-Ionizing Radiation (NIR) levels and assessing the network performance in terms of coverage probability and data throughput.

As the demand for wide bandwidth at millimeter-wave frequencies increases, it is necessary to consider any potential impact on the organic and biological systems of humans. This becomes crucial with massive MIMO and beamforming techniques in next-generation networks, which provide substantial gains in signal power to improve the network performance. To assess the potential radiation exposure in the 6G network, this study employed the IEEE C95.1-2005 standard, aiming to achieve a clean and environmentally friendly mobile network. In this context, a DBS network with low transmit power is suggested as a way to reduce the NIR exposure to nearby users. The performance of both mMIMO and DBS networks is evaluated in terms of radiation, spectral efficiency, and data throughput.

The findings suggest that, at the mmWave band, the DBS architecture offers the most favorable option for next-generation mobile networks. This is due to the notable reduction in radiation levels compared to the high associated power of massive MIMO. Additionally, the LPN with DBS architecture demonstrates that the reduction in radiation exposure can be accomplished without compromising the QoS provision in the network. In summary, this study advocates for the adoption of a DBS network with an LPN as a more suitable solution for 6G deployment at the mmWave band. The implementation of such an architecture can effectively minimize radiation exposure while ensuring a robust and efficient 6G network performance, meeting the growing demands of modern wireless communication systems.

Author Contributions: Conceptualization, N.A.-F. and O.Y.A.; Methodology, N.A.-F. and O.Y.A.; Validation, N.A.-F. and O.Y.A.; Investigation, N.A.-F.; Data curation, N.A.-F.; Writing—review & editing, O.Y.A.; Supervision, O.Y.A. All authors have read and agreed to the published version of the manuscript.

Funding: The authors would like to express their gratitude to The University of Salford for sponsoring and funding this research.

Data Availability Statement: Data are contained within the article.

Conflicts of Interest: The authors have no conflict of interest to declare.

References

1. Ericsson. Mobile Data Traffic. Ericsson Mobility Visualizer. 2023. Available online: <https://www.ericsson.com/en/reports-and-papers/mobility-report> (accessed on 15 November 2023).
2. ITU. Minimum Requirements Related to Technical Performance for IMT-2020 Radio Interface(s). Work. Party 5D, vol. November, no. 5D/TEMP/300(Rev.1). 2017. pp. 1–148. Available online: <https://www.itu.int/pub/R-REP-M.2410-2017> (accessed on 3 January 2024).
3. Ferrag, M.A.-H.M.A.; Debbah, M. Generative AI for Cyber Threat-Hunting in 6G-enabled IoT Networks. In Proceedings of the IEEE/ACM 23rd International Symposium on Cluster, Cloud and Internet Computing Workshops (CCGridW), Bangalore, India, 1–4 May 2023; pp. 16–25.
4. Al-falahy, N.; Alani, O.Y.K. Millimetre Wave Frequency Band as a Candidate Spectrum for 5G Network Architecture: A Survey. *Phys. Commun.* **2019**, *32*, 120–244. [CrossRef]
5. Al-falahy, N.; Alani, O.Y.K. Reducing the Exposure to Millimetre Wave Radiation Using Distributed Base Stations in C-RAN Architecture. In Proceedings of the 10th Computer Science & Electronic Engineering Conference (CEEC), Colchester, UK, 19–21 September 2018; pp. 1–6.
6. LEXNET. LEXNET Project: Low EMF Exposure Networks. 2018. Available online: <http://www.lexnet.fr> (accessed on 15 March 2018).
7. Wu, T.; Rappaport, T.S.; Collins, C.M. The Human Body and Millimeter-Wave Wireless Communication Systems: Interactions and Implications. In Proceedings of the IEEE International Conference on Communications, London, UK, 8–12 June 2015; pp. 2423–2429.
8. *IEEE Std C95.1-2005*; IEEE Standard for Safety Levels with Respect to Human Exposure to Radio Frequency Electromagnetic Fields, 3 kHz to 300 GHz. IEEE: Piscataway, NJ, USA, 2006; pp. 1–238. [CrossRef]

9. International Commission on Non-Ionizing Radiation Protection (ICNIRP). Guidelines for limiting exposure to time-varying electric, magnetic, and electromagnetic fields (up to 300 GHz). *Health Phys.* **1998**, *74*, 494–522. [CrossRef]
10. Al-Falahy, N.; Alani, O. Technologies for 5G Networks: Challenges and Opportunities. *IEEE IT Prof.* **2017**, *19*, 12–20. [CrossRef]
11. Modenese, A.; Gobba, F. Occupational Exposure to Non-Ionizing radiation. Main effects and criteria for health surveillance of workers according to the European Directives. In Proceedings of the IEEE International Conference on Environment and Electrical Engineering (EEEIC), Madrid, Spain, 9–12 June 2020; pp. 1–6.
12. Rappaport, T.S.; Sun, S.; Mayzus, R.; Zhao, H.; Azar, Y.; Wang, K.; Wong, G.N.; Schulz, J.K.; Samimi, M.; Gutierrez, F. Millimeter Wave Mobile Communications for 5G Cellular: It Will Work ! *IEEE Access* **2013**, *1*, 335–349. [CrossRef]
13. Al-falahy, N.; Alani, O. The Impact of Base Station Antennas Configuration on the Performance of Millimetre Wave 5G Networks. In Proceedings of the Ninth International Conference on Ubiquitous and Future Networks (ICUFN), Milan, Italy, 4–7 July 2017; pp. 636–641.
14. G-PPP. 5G Infrastructure Public Private Partnership. 2018. Available online: <https://5g-ppp.eu/> (accessed on 20 March 2018).
15. Siegel, P.; Pikov, V. Impact of Low Intensity Millimeter-Waves on Cell Membrane Permeability. In Proceedings of the 34th International Conference on Infrared, Millimeter, and Terahertz Waves, IRMMW-THz, Busan, Republic of Korea, 21–25 September 2009; p. 978.
16. Foster, K.; Colombi, D. Thermal response of tissue to RF exposure from canonical dipoles at frequencies for future mobile communication systems. *Electron. Lett.* **2017**, *53*, 360–362. [CrossRef]
17. Guraliuc, A.R.; Zhadobov, M.; Sauleau, R.; Marnat, L.; Dussopt, L. Near-Field User Exposure in Forthcoming 5G Scenarios in the 60 GHz Band. *IEEE Trans. Antennas Propag.* **2017**, *65*, 6606–6615. [CrossRef]
18. Basikolo, T.; Yoshida, T.; Sakurai, M. Electromagnetic field exposure evaluation for 5G in millimeter wave frequency band. In Proceedings of the IEEE International Symposium on Antennas and Propagation and USNC-URSI Radio Science Meeting, APSURSI 2019, Atlanta, GA, USA, 7–12 July 2019; pp. 1523–1524. [CrossRef]
19. Li, K.; Sasaki, K.; Watanabe, S. EMF Exposure from 5G Equipment at Millimeter Wave Frequencies. In Proceedings of the IEEE International Workshop on Electromagnetics: Applications and Student Innovation Competition, iWEM 2018, Nagoya, Japan, 29–31 August 2018; p. 1. [CrossRef]
20. Colombi, D.; Thors, B.; Tornevik, C.; Balzano, Q. RF Energy Absorption by Biological Tissues in Close Proximity to Millimeter-Wave 5G Wireless Equipment. *IEEE Access* **2018**, *6*, 4974–4981. [CrossRef]
21. Tirkel, A.Z.; Lai, J.C.S.; Evans, T.A.; Rankin, G.A. Effects of millimeter wave exposure on termite behavior. In Proceedings of the Progress in Electromagnetics Research Symposium, Marrakesh, Morocco, 20–23 March 2011; pp. 1581–1585.
22. Wang, H. A Unified Quantitative Index to Assess Non-ionizing Radiation Safety. *IEEE Consum. Electron. Mag.* **2022**, *12*, 84–93. [CrossRef]
23. Sun, Y.; An, K.; Zhu, Y.; Zheng, G.; Wong, K.K.; Chatzinotas, S.; Ng, D.W.K.; Guan, D. Energy-Efficient Hybrid Beamforming for Multilayer RIS-Assisted Secure Integrated Terrestrial-Aerial Networks. *IEEE Trans. Commun.* **2022**, *70*, 4189–4210. [CrossRef]
24. Lin, Z.; Niu, H.; An, K.; Hu, Y.; Li, D.; Wang, J.; Al-Dhahir, N. Pain without Gain: Destructive Beamforming from a Malicious RIS Perspective in IoT Networks. *IEEE Internet Things J.* **2023**. early access. [CrossRef]
25. Sun, Y.; An, K.; Zhu, Y.; Zheng, G.; Wong, K.K.; Chatzinotas, S.; Yin, H.; Liu, P. RIS-Assisted Robust Hybrid Beamforming against Simultaneous Jamming and Eavesdropping Attacks. *IEEE Trans. Wirel. Commun.* **2022**, *21*, 9212–9231. [CrossRef]
26. Ansal, K.A.; Jose, D.S.; Rajan, R.K. Review on Biological Effect of Electromagnetic Radiation. In Proceedings of the 2018 International Conference on Circuits and Systems in Digital Enterprise Technology, ICCSDET 2018, Kottayam, India, 21–22 December 2018; pp. 1–5. [CrossRef]
27. Kour, H.; Jha, R.K. EM Radiation Reduction in WCN: Towards Safe Generations. In Proceedings of the 2020 International Conference on Communication Systems and Networks, Comsnets 2020, Bangalore, India, 7–11 January 2020; pp. 559–562. [CrossRef]
28. El Amrani, L.; Mazri, T.; Hmina, N. The Specific Absorption Rate induced in human organs due Ionizing and Non Ionizing Radiations exposure. In Proceedings of the 6th International Conference on Wireless Networks and Mobile Communications (WINCOM), Marrakesh, Morocco, 16–19 October 2018; pp. 1–4. [CrossRef]
29. Kour, H.; Jha, R.K. Electromagnetic Radiation Reduction in 5G Networks and beyond Using Thermal Radiation Mode. *IEEE Trans. Veh. Technol.* **2020**, *69*, 11841–11856. [CrossRef]
30. Ajibare, A.T.; Ramotsoela, D.; Akinyemi, L.F.; Oladejo, S.O. RF EMF Radiation Exposure Assessment of 5G Networks: Analysis, Computation and Mitigation Methods. In Proceedings of the 2021 IEEE AFRICON, Arusha, Tanzania, 13–15 September 2021; pp. 1–7. [CrossRef]
31. Ramos, V.; Suárez, S.D.; Marina, P.; Febles, V.M.; Rabassa, L.E.; Hernández, J. Survey of RF Electromagnetic Field Exposure in a Public Health Research Environment. In Proceedings of the International Symposium on Electromagnetic Compatibility—EMC Europe, Kraków, Poland, 4–8 September 2023; pp. 1–11. [CrossRef]
32. Kharel, B.; Lopez, O.L.A.; Mahmood, N.H.; Alves, H.; Latva-Aho, M. Fog-RAN Enabled Multi-Connectivity and Multi-Cell Scheduling Framework for Ultra-Reliable Low Latency Communication. *IEEE Access* **2022**, *10*, 7059–7072. [CrossRef]
33. Tinini, R.I.; Batista, D.M.E.; Figueiredo, G.B.; Tornatore, M.; Mukherjee, B. Energy-Efficient vBBU Migration and Wavelength Reassignment in Cloud-Fog RAN. *IEEE Trans. Green Commun. Netw.* **2021**, *5*, 18–28. [CrossRef]

34. Cleveland, J.R.F.; Sylvar, D.M.; Ulcek, J.L. Evaluating Compliance with FCC Guidelines for Human Exposure to Radiofrequency Electromagnetic Fields. *OET Bull.* **1997**, *65*, 1–84.
35. Federal Communications Commission (FCC). Radio Spectrum Allocation. 2018. Available online: www.fcc.gov/engineering-technology/policy-and-rules-division/general/radio-spectrum-allocation (accessed on 6 April 2018).
36. International Telecommunication Union (ITU). World Radiocommunication Conferences (WRC). 2018. Available online: <https://www.itu.int/en/ITU-R/conferences/wrc> (accessed on 6 April 2018).
37. Federal Communications Commission (FCC). *Use of Spectrum Bands Above 24 GHz for Mobile Radio Services*; Technical Report, no. GN Docket No. 14-177; Federal Communications Commission (FCC): Washington, DC, USA, 2017; pp. 1–137.
38. Roh, W.; Seol, J.-Y.; Park, J.; Lee, B.; Lee, J.; Kim, Y.; Cho, J.; Cheun, K.; Aryanfar, F. Millimeter-Wave Beamforming as an Enabling Technology for 5G Cellular Communications: Theoretical Feasibility and Prototype Results. *IEEE Commun. Mag.* **2014**, *52*, 106–113. [[CrossRef](#)]
39. Boccardi, F.; Heath, R.W., Jr.; Lozano, A.; Marzetta, T.L.; Popovski, P. Five Disruptive Technology Directions for 5G. *IEEE Commun. Mag.* **2014**, *52*, 74–80. [[CrossRef](#)]
40. Ofcom. *Update on 5G Spectrum in the UK*; Ofcom: London, UK, 2017; pp. 1–19.
41. Nokia. Spectrum for 6G Explained. 2023. Available online: <https://www.nokia.com/about-us/newsroom/articles/spectrum-for-6g-explained/> (accessed on 15 December 2023).
42. Rappaport, T.S.; Xing, Y.; Kanhere, O.; Ju, S.; Madanayake, A.; Mandal, S.; Alkhateeb, A.; Trichopoulos, G.C. Wireless communications and applications above 100 GHz: Opportunities and challenges for 6g and beyond. *IEEE Access* **2019**, *7*, 78729–78757. [[CrossRef](#)]
43. ITU. World Radiocommunication Conference. 2023. Available online: <https://www.itu.int/wrc-23/> (accessed on 18 December 2023).
44. Lin, Z.; Lin, M.; Champagne, B.; Zhu, W.P.; Al-Dhahir, N. Secrecy-Energy Efficient Hybrid Beamforming for Satellite-Terrestrial Integrated Networks. *IEEE Trans. Commun.* **2021**, *69*, 6345–6360. [[CrossRef](#)]
45. Prabu, R.T.; Benisha, M.; Bai, V.T.; Yokesh, V. Millimeter Wave for 5G Mobile Communication Application. In Proceedings of the International Conference on Advances in Electrical, Electronics, Information, Communication and Bio-Informatics (AEEICB16), Chennai, India, 27–28 February 2016; pp. 1–5.
46. Cui, Z.; Zhang, P.; Pollin, S. 6G Wireless Communications in 7–24 GHz Band: Opportunities, Techniques, and Challenges. *arXiv* **2023**, arXiv:2310.06425.
47. Huang, J.; Cao, Y.; Raimundo, X.; Cheema, A.; Salous, S. Rain Statistics Investigation and Rain Attenuation Modeling for Millimeter Wave Short-Range Fixed Links. *IEEE Access* **2019**, *7*, 156110–156120. [[CrossRef](#)]
48. Rajagopal, S.; Abu-Surra, S.; Malmirchegini, M. Channel Feasibility for Outdoor Non-Line-of-Sight mmWave Mobile Communication. In Proceedings of the IEEE Vehicular Technology Conference (VTC Fall) 2012, Quebec City, QC, Canada, 3–6 September 2012; pp. 1–6.
49. Rappaport, T.S.; Gutierrez, F.; Ben-dor, E.; Murdock, J.N.; Qiao, Y.; Tamir, J.I. Broadband Millimeter-Wave Propagation Measurements and Models Using Adaptive-Beam Antennas for Outdoor Urban Cellular Communications. *IEEE Trans. Antennas Propag.* **2013**, *61*, 1850–1859. [[CrossRef](#)]
50. 3GPP Technical Report 38.901. Technical Specification Group Radio Access Network; Study on channel model for frequencies from 0.5 to 100 GHz. 2017. Available online: <https://www.3gpp.org/dynareport/38901.htm> (accessed on 3 January 2024).
51. Al-Falahy, N.; Alani, O. Improved Capacity and Fairness of Massive Machine Type Communications in Millimetre Wave 5G Network. *Computers* **2018**, *7*, 16. [[CrossRef](#)]
52. Ozuomba, S.; Johnson, E.H.; Udoiwod, E.N. Application of Weissberger Model for Characterizing the Propagation Loss in a *Gliricidia sepium* Arboretum. *Univ. J. Commun. Netw.* **2018**, *6*, 18–23. [[CrossRef](#)]
53. Marcus, M.; Pattan, B. Millimeter Wave Propagation: Spectrum Management Implications. *IEEE Microw. Mag.* **2005**, *6*, 54–62. [[CrossRef](#)]
54. Curry, T.S.; Dowdey, J.E.; Murry, R.C. *Christensen's Physics of Diagnostic Radiology*, 4th ed.; Lea & Febiger, U.S.: Philadelphia, PA, USA, 1990.
55. Zhadobov, M.; Chahat, N.; Sauleau, R.; Le Qument, C.; Le Drean, Y. Millimeter-wave interactions with the human body: State of knowledge and recent advances. *Int. J. Microw. Wirel. Technol.* **2011**, *3*, 237–247. [[CrossRef](#)]
56. Al-Falahy, N.; Alani, O. Supporting Massive M2M Traffic in the Internet of Things Using Millimetre Wave 5G Network. In Proceedings of the 9th Computer Science & Electronic Engineering Conference (CEEC), Colchester, UK, 27–29 September 2017; pp. 83–88.

Disclaimer/Publisher's Note: The statements, opinions and data contained in all publications are solely those of the individual author(s) and contributor(s) and not of MDPI and/or the editor(s). MDPI and/or the editor(s) disclaim responsibility for any injury to people or property resulting from any ideas, methods, instructions or products referred to in the content.